Nanoscale

Accepted Manuscript

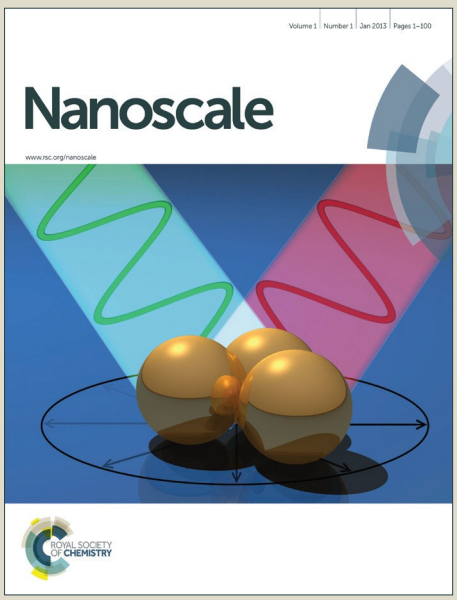

ROYAL SOCIETY OF CHEMISTRY

www.rsc.org/nanoscale

Table of contents entry

Artificial nacre-like papers with excellent mechanical and thermally conductive properties were fabricated via vacuum-assisted self-assembly of noncovalent functionalized boron nitride nanosheets and poly (vinyl alcohol).

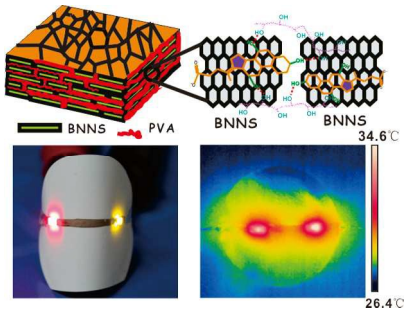

Cite this: DOI: 10.1039/c0xx00000x

www.rsc.org/xxxxxx

ARTICLE TYPE

Artificial Nacre-like Papers Based on Noncovalent Functionalized Boron Nitride Nanosheets with Excellent Mechanical and Thermally Conductive Properties

Xiaoliang Zeng,[‡a] Lei Ye,[‡b] Shuhui Yu,[a] Hao Li,[b] Rong Sun*[a], and Jianbin Xu*[b] and Ching-Ping Wong[b]

Received (in XXX, XXX) Xth XXXXXXXXX 20XX, Accepted Xth XXXXXXXXX 20XX
DOI: 10.1039/b000000x

Inspired by the nano/microscale hierarchical structure and precise inorganic/organic interface of natural nacre, we fabricate artificial nacre-like papers based on noncovalent functionalized boron nitride nanosheets (NF-BNNSs) and poly(vinyl alcohol) (PVA) via vacuum-assisted self-assembly technique. The artificial nacre-like papers exhibit excellent tensile strength (125.2 MPa), on par with that of the natural nacre, and moreover display a 30 % higher toughness (2.37 MJ m^{-3}) than that of the natural nacre. These excellent mechanical properties result from an ordered 'brick-and-mortar' arrangement of NF-BNNSs and PVA, in which the long-chain PVA molecules act as the bridge to link NF-BNNSs via hydrogen bonds. The resulting papers also render high thermal conductivity (6.9 W m^{-1} K^{-1}), and reveal the superiority as flexible substrates to support light-emitting-diode chips. The combined mechanical and thermal properties make the materials highly desirable as flexible substrates for next-generation commercial portable electronics.

Introduction

As graphene analogues, boron nitride nanosheets (BNNSs) possessing a number of remarkable properties, such as a wide energy band gap,[1] high resistance to oxidation,[2] good chemical inertness,[3] electrical-insulating properties,[4] high surface area,[5] and high thermal conductivity,[6] have attracted ever-growing attention in several fields in the past few years.[4, 7, 8] However, to utilize these excellent properties for achieving their applications in industry, the key challenge is how to assemble the BNNSs to form macroscopic materials that have exciting properties of their nanometer-scale building blocks. The assembly of nanosheets into free-standing paper-like or film-like structure has been considered to be an effective way to address this problem. For example, the assembly of graphene into free-standing paper-like materials[9, 10] has been demonstrated extraordinary properties,[11-13] which can be applicable to electrical packaging,[14] sensors,[15] catalysis,[16] absorption agents,[17] substrate,[18] and energy storage and conversion.[19, 20] However, the free-standing BNNSs papers prepared by the simple and direct assembly[21, 22] usually lack sufficient toughness and strength, resulting in catastrophic and unpredictable failure, which greatly limits their range of applications. BNNSs papers with an exceptional toughness and strength are thus in great demand.

Unfortunately, high strength and high toughness are usually mutually exclusive in engineering materials. In the process of evolution, nature has found its ingenious way around this dilemma by combining brittle minerals and organic molecules into hybrid composites with outstanding fracture resistance and structural capabilities.[23, 24] The most famous example is probably the natural nacre, whose remarkably high toughness (1.80 MJ m^{-3}) and mechanical strength (80-135 MPa) have been widely recognized.[25, 26] The layered arrangement of platelet-shaped $CaCO_3$ and proteins building into a "bricks-and-mortar" structure is crucial to contribute to nacre's outstanding mechanical properties.[27] Inspired by nacre's intrinsic relationship between the structure and mechanical properties, many scientists have fabricated a number of different artificial nacre-like nanocomposite papers,[28-32] with cationic,[33, 34] small molecules,[35, 36] and polymers[11, 37, 38] as mortars to bridge the nanosheets. Thus, such progress is fuelling a growing conviction that mimicking the architecture of natural nacre seems to be a viable approach to design BNNSs papers with gratified strength and toughness.

Herein, artificial nacre-like papers were fabricated based on noncovalent functionalized BNNSs (NF-BNNSs) and poly (vinyl alcohol) (PVA) through a vacuum-filtration-induced self-assembly technique. In contrast to the BNNSs in polymer composites reported previously,[39-42] these NF-BNNSs are the matrix phase, acting the similar function of the "brick" in the nacre structure. The alignment of the NF-BNNSs is successfully constructed by the link of interlayer bridges (PVA) in this nacre-like structure, resulting in excellent tensile strength and toughness. Furthermore, the interlayer bridges formed by PVA could offer additional benefit to improvement of thermal conductivity. By considering the excellent mechanical properties and high thermal conductivity, we also demonstrate that the obtained nacre-like BNNSs papers can be used as flexible substrates to support light-emitting-diode (LED) chips. The effective heat dissipation of the nacre-like papers does significantly decrease the LED operation

temperature, so as to improve the reliability and lifetime of LEDs. To the best of our knowledge, although numerous examples on nacre-like materials have arisen, there is no report on nacre-like BNNSs materials, and not to mention their potential application.

Experimental Section

Preparation of NF-BNNSs

NF-BNNSs were obtained using combined low-energy ball milling and sonication, which is a facile, efficient, and scalable method, as Yao *et al.*'s report.[22] The initial 2.0 g h-BN powders, and 200 mL 0.05 wt% surfactant sodium cholate (SC) water solutions were loaded in a sealed polytetrafluoroethylene ball milling tank with 400 zirconia balls (2 mm in diameter). The rotation speed of the planetary mill was set at 200 rpm to generate rolling actions of the balls, which apply shearing forces on materials. After ball milling for 12 h, the solutions were then sonicated for 2h. Finally, the solutions were centrifutated at 2000 rpm for 25 minutes to remove aggregates, and NF-BNNSs solution with 2.3 mg mL^{-1} was obtained. The NF-BNNSs solution was then filtrated to remove the excess of SC. This procedure was repeated once more to ensure any free SC was removed. The filter was dispersed once again in water and sonicated (30 min).

Fabrication of NF-BNNSs-PVA papers

PVA was dissolved in deionized water at 80 °C and stirred for 30 min under magnetic stirrer to obtain 10 wt% PVA solution, which was then dropped into the NF-BNNSs suspension during stirring. The mixture of NF-BNNSs and PVA was kept stirring for 60 min and placed in a bath sonification for 60 min to form a uniform NF-BNNSs-PVA suspension. The prepared NF-BNNSs-PVA suspension was filtered through a vacuum system equipped with a cellulose acetate membrane (50 mm in diameter, 0.22 μm pore size). The obtained wet paper was peeled from the filter papers and dried at 50 °C. Unless specifically stated, NF-BNNSs papers with a thickness of around 0.03 mm were used for all measurements reported in this work. The content of PVA molecules in NF-BNNSs-PVA papers was varied from 0% to 10 wt%. It should be noted that because a little PVA (~1 wt% confirmed by TGA) was lost in the beginning of filtration, 1 wt% PVA was supplemented to ensure the weight ratio.

Characterization

Atomic force microscopy (AFM) image of NF-BNNSs was taken in the tapping mode by carrying out on a Nanoscope IIIa Multimode apparatus (Veeco Instruments). Sample was prepared by spin-coating from diluted aqueous solutions onto freshly exfoliated mica substrates at 2000 rpm. The average thickness of NF-BNNSs was obtained by averaging the testing values of repeated measurements. Dynamic light scattering (DLS) was utilized to determine the particle size in the water suspension obtained by using Mastersizer 3000 Laser Diffraction Particle Size Analyzer. Raman spectra of BNNSs were obtained from 1000 to 2000 cm^{-1} using a Raman spectrometer (Renishawin Via Raman microscope, excitation at 514 nm). The Fourier transform infrared spectroscopy (FTIR) spectra were obtained on a Bruker Vertex 70 with pure KBr as the background from 400 and 4000 cm^{-1}. transmission electron microscopy (TEM) images were taken by transmission electron microscopy (G2 F20, FEI Tecnai) with an accelerating voltage of 200 kV. TEM sample was prepared by dropping NF-BNNSs solution on the copper grid, following by drying. SEM images of NF-BNNSs papers were obtained using a field-emission scanning electronmicroscope (Nova NanoSEM 450, FEI) with 10 kV accelerating voltage. The thermal stability of the BNNSs was characterized by thermogravimetric analysis (TGA, Q600, TA Instruments). The measurements were conducted under air atmosphere at a flow rate of 100 mL min^{-1} over a temperature range of 30-900 °C with a ramp rate of 10 °C min^{-1}. Static uniaxial in-plane tensile tests were conducted with a dynamic mechanical analyzer (DMA Q800, TA Instruments). The samples were cut with a razor into rectangular strips (3-6 mm wide and 20 mm long) for mechanical testing and were gripped using a film tension clamp with a clamp compliance of about 0.2 μm N^{-1}. All tensile tests were conducted in controlled strain rate mode with a preload of 0.01N and a force ramp rate of 0.5 N min^{-1}. The ultimate tensile strength and ultimate strain (ε_{max}) were extracted from the curve just before the failure. Young's modulus (E) was obtained from the slope of the linear fit in the initial section of the curve (0.1% strain). The in-plane thermal conductivities were measured through the laser flash technique (NETZXCH, LFA 447 NanoFlash). The laser flashtechnique has been generally known as the standard and popular method for measuring in-plane thermal conductivity. In-plane thermal conductivity (λ) was calculated using Equation (1):

$$\lambda = \rho \cdot C_P \cdot D \quad (1)$$

where ρ is the density of the papers, and C_p is the specific heat capacity, and D is the thermal diffusivity. Please see Supporting Information for detailed procedures and results of in-plane thermal conductivity.

Results and Discussion

NF-BNNSs were obtained using the method combined low-energy ball milling and sonication technique, as illustrated in Figure 1a, through a previously reported method.[22] Sodium cholate (SC) was used to achieve noncovalent functionalization of BNNSs, because it has a strong affinity with the basal plane of BNNSs[43] and graphene[44] via van der Waals, according to the previous studies. Indeed, the milky NF-BNNSs are stable in aqueous over several weeks, but the raw h-BN exhibits the limited solubility in water. Figure 1b shows the typical AFM image of NF-BNNSs with the size ranging from 50-500 nm. DLS (Figure S2, ESI†) analysis shows a mean diameter of 200 nm. The height profile in Figure 2b indicates that the average thickness of the BNNSs is around 3 nm, confirming that the obtained NF-BNNSs are few-layer. The TEM image (Figure S1, ESI†) also presents the few-layers (<10) NF-BNNSs, which agress with AFM characterization. Moreover, a red shift of 3 cm^{-1} in the E_{2g} phonon mode at 1364 cm^{-1} is observed by Raman spectroscope analysis (Figure S3, ESI†), also indicating that the NF-BNNSs are few-layers.[45] The noncovalent functionalization of BNNSs is verified by FTIR and TGA. Compared with the raw h-BN and SC, the FTIR spectrum of the NF-BNNSs exhibits the additional -OH, C-H, and weaken C-O bands in 3450, 2962-2855 and 1000-1200 cm^{-1} regions, respectively, as displayed in Figure 1c. The result indicates that noncovalent functionalization of BNNSs occurs via van der Waals binding, which is consistent with the report by Coleman *et al.*'s.[43] The TGA reveals that a

mass loss of 6 wt% is recorded for the NF-BNNSs, while the reference sample of the raw h-BN just demonstrates a 1 wt% mass loss, indicating that the quantity of SC is estimated to be 5 wt% in the NF-BNNSs (Figure S4, ESI†).

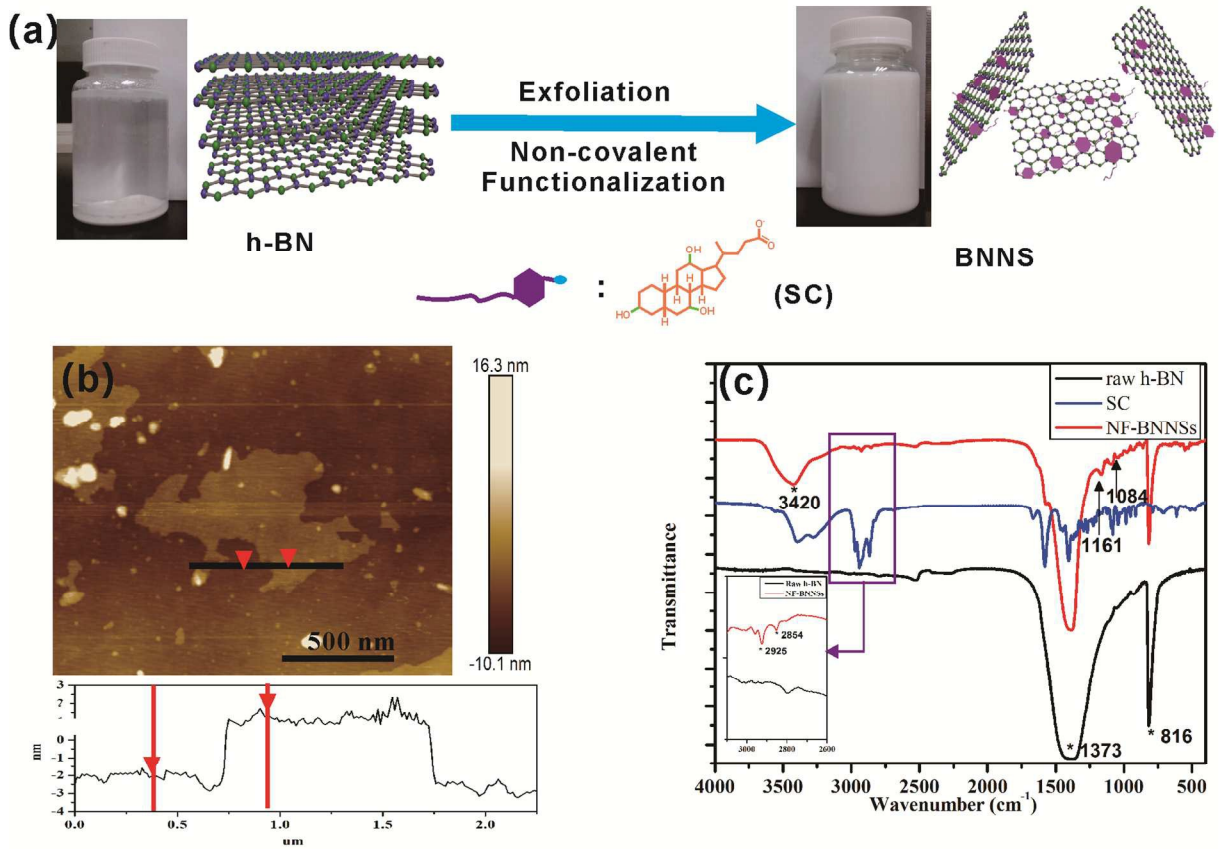

Figure 1. Preparation and characterization of NF-BNNSs. (a) The illustration of the exfoliation and functionalization process of NF-BNNSs, (b) AFM image and height profiles of NF-BNNSs, (c) FTIR spectra of NF-BNNSs and pristine h-BN. The inset is the expanded scale of the FTIR region 2600-3100 cm^{-1}.

NF-BNNSs-PVA papers were obtained based on aqueous suspension of NF-BNNSs and PVA, via a vacuum-filtration-induced self-assembly technique. The typical 'brick-and-mortar' model of our artificial nacre-like papers is shown in Figure 2a. Because of the existence of the hydrogen-bonds (H-bonds) between the hydroxyl groups of PVA and SC, PVA is to link the neighbored NF-BNNSs (Figure 2a, below), revealing the similar function of biopolymers in the natural nacre.[46] The microstructure of the NF-BNNSs-PVA paper with 6 wt% PVA is characterized by SEM and compared with that of natural nacre. For natural nacre (Figure 2b and d), the ordered 'brick-and-mortar' arrangement of organic and inorganic layers and long-range order of platelets are observed, which are regarded as the most essential structure feature that leads to excellent mechanical properties. Correspondingly, the NF-BNNSs-PVA paper with excellent flexibility (Figure 2c) displays the similar well-packed layered structures (Figure 2g). However, the packing of NF-BNNSs platelets presents short-range order, and the long-range order is not as perfect. Observations of the interfaces between platelets (Figure 2h) reveal the presence of a polymer phase used as bridges, mimicking the organic layer in natural nacre (Figure 2e). In additon, the thickness of BNNSs seems to increase to about 50 nm due to the restacking of few-layer BNNSs. The surface morphology of the NF-BNNSs-PVA paper (Figure 2i) reveals its microscopically flat surfaces with nanoscale roughness, which is also similar to that of natural nacre (Figure 2f). X-ray diffraction (XRD) is employed to investigate the structure of NF-BNNSs-PVA paper. The interlayer distance between BNNSs of the NF-BNNSs-PVA paper increases to 3.94 Å (2θ=22.52°) from 3.33 Å (2θ=26.76°) for the pure BNNSs paper, suggesting PVA adsorption on the NF-BNNSs (Figure S4, ESI†). In addition, the pure BNNSs paper can be re-dispersed into water with just a mild shake or resting for 24 hours, generating a homogeneous BNNSs suspension (Figure S6, ESI†). In contrast, the NF-BNNSs-PVA paper cannot be re-dispersed in water even after keeping a longer time. The reason may be that the PVA molecules link the NF-BNNSs sheets together like the mortar in a "bricks-and-mortar" structure, thereby preserving NF-BNNSs-PVA paper structure in aqueous solution. The above results confirm that our artificial nacre has a nacre-like structure, in which the NF-BNNSs are stacked and glued together effectively by PVA adhesive.

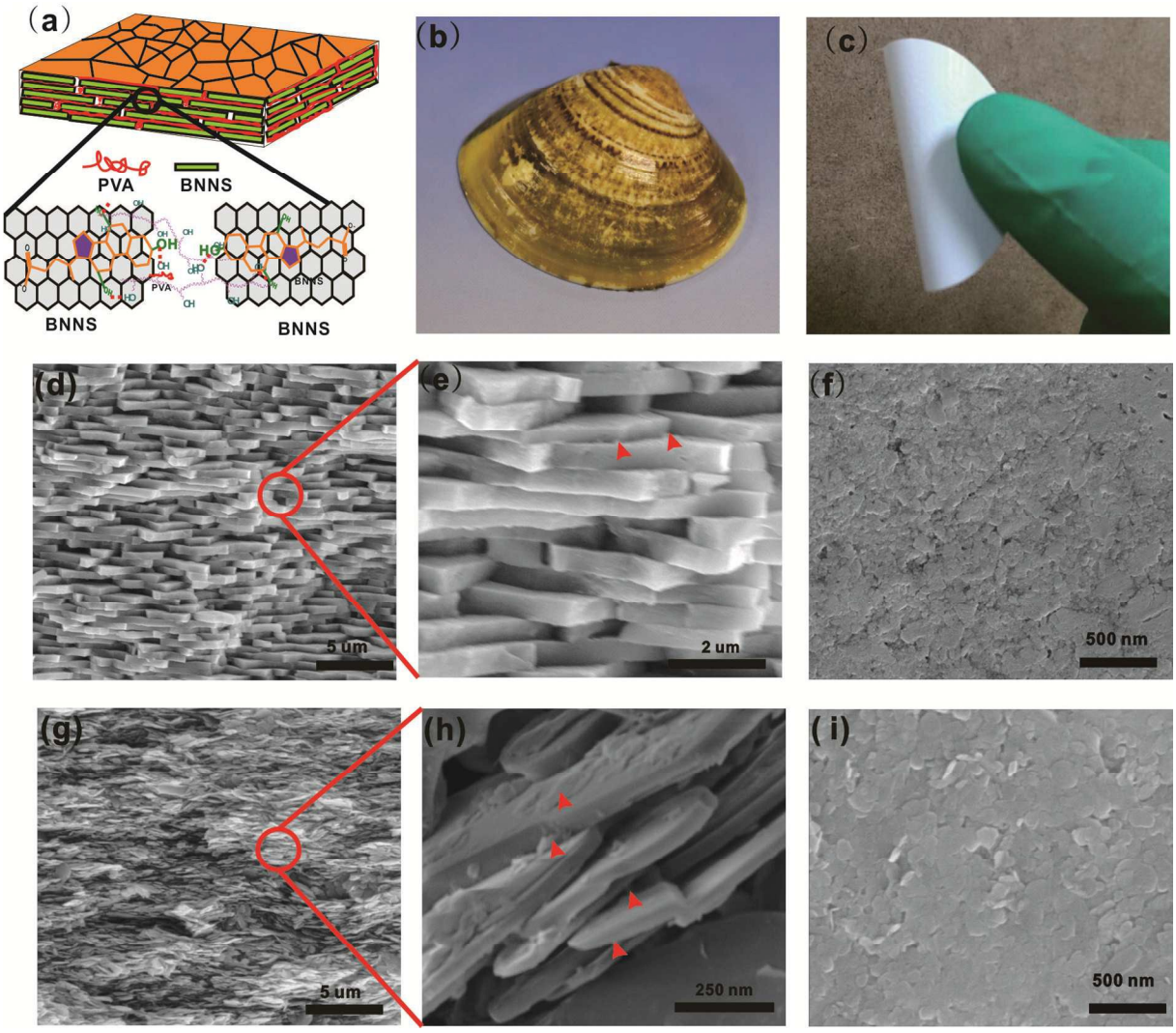

Figure 2. Microstructural comparison of NF-BNNSs-PVA paper (6 wt% PVA) with natural nacre. (a) Schematic illustration of the construction of the artificial nacre-like NF-BNNSs-PVA paper and the function of PVA in the paper. (b, c) The optical image of natural nacre (b) and NF-BNNSs-PVA paper (c). (d-f) SEM cross-sectional (d, e) and surface morphology (f) of natural nacre. (g-i) SEM cross-sectional (g, h) and surface morphology (i) of the NF-BNNSs-PVA paper. Red arrows in e and h indicate the bridges between platelets.

To explore the relationship between the mechanical properties and the amount of PVA, we fabricated the NF-BNNSs papers with a range of PVA loadings, which is confirmed by TGA (Figure S7, ESI†). The typical stress-strain curves of the NF-BNNSs-PVA papers are shown in Figure 3a, and their tensile strength, Young's modulus and toughness are summarized in Table S1. It should be noted that the pure NF-BNNSs paper is too fragile to carry out the tensile test. As shown in Figure 3a and Table S1, the mechanical properties of the NF-BNNSs-PVA papers increase with the PVA loadings, which may be due to the increase of the H-bonds. When 6 wt% PVA are grafted on the NF-BNNSs, the tensile strength is increased to 125.2±5.1 MPa, which is comparable to that of natural nacre, while the toughness is dramatically raised to 2.37±0.2 MJ m^{-3}, which is about 30% higher than that of the natural nacre.[28] When more PVA is added (10 wt%), the tensile strength and toughness of NF-BNNSs-PVA paper are slightly increased to 135.5±4.7 MPa and 2.99±0.3 MJ m^{-3}, respectively, but the Young's modulus decreases to 5.43±1.0 GPa. This is likely to be attributed to the harm of intercalating impurities to the Young's modulus, resulted by the excess PVA without interacting with SC on BNNSs.

The excellent mechanical properties of the NF-BNNSs-PVA papers are attributed to the layered hierarchical structure and the unique cross-linking with the PVA via H-bonds. Detailed microstructural analysis is performed to understand the intrinsic factors to improve the mechanic properties. As shown in surface morphology of the pure NF-BNNSs paper (Figure 3b), plentiful air gaps are observed, suggesting a poor interaction between the NF-BNNSs, and thus leading to low mechanical properties. After the addition of PVA, the air gaps are disappeared (Figure 3c), indicating an enhanced interfacial strength between NF-BNNSs via H-bonds. In this way, energy dissipation via cooperative sliding of NF-BNNSs pervades through a larger volume than that of the pure BNNSs paper, leading to better mechanical properties. A breaking-down process is proposed to further understand the function of PVA, by combining the fracture morphology analysis. As depicted in Figure 3d, the

PVA molecules are grafted on the NF-BNNSs via H-bonds to form the intercross-linked networks in the layered structure. After the force loading, the NF-BNNSs firstly slide against each other, and subsequently, the PVA long chains acted as bridges between NF-BNNSs are stretched along the sliding direction to dissipate a large amount of the loading energy. This hypothesis is demonstrated by the fracture morphology of SEM (Figure 3e), in which the fractured NF-BNNSs linked with PVA bridges are observed. Further increasing the loading strength (Figure 3f and g), the H-bonds between the PVA and the NF-BNNSs are broken, simultaneously resulting in NF-BNNSs pulling out from bricks.

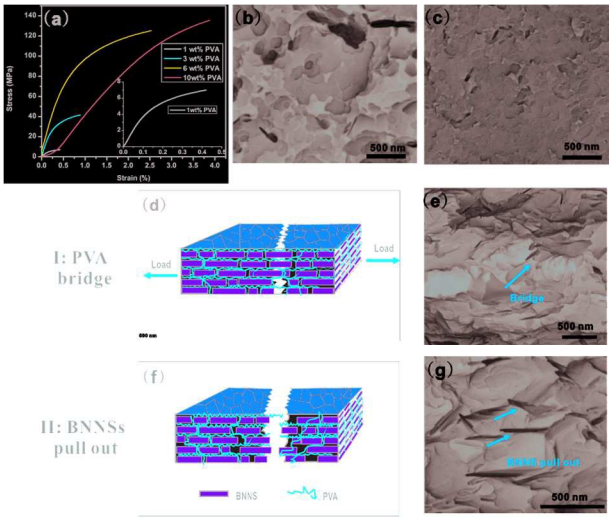

Figure 3. Mechanical properties and fracture mechanism of the NF-BNNS-PVA papers**.** (a) Stress-strain curves of the NF-BNNSs-PVA papers as a function of PVA contents. (b, c) SEM surface morphology of the pure NF-BNNSs paper (b) and the NF-BNNSs-PVA paper (6 wt% PVA)(c). (d) Simplified structural schematics, showing that the PVA acts as bridges to dissipate the crack energy. (e) SEM fracture morphology of the NF-BNNSs-PVA paper under (d). (f) The overall fracture of NF-BNNSs-PVA paper finally fails under NF-BNNSs pull-out mode. (g) SEM fracture morphology of the NF-BNNSs-PVA paper.

The importance of H-bonds for improving the mechanical properties is further demonstrated by the observation of drastic variance in mechanical properties between multi-H-bonds and few-H-bonds NF-BNNSs papers. Poly (methyl methacrylate) (PMMA) is chosen as hydrophobic polymer to prepare few-H-bonds NF-BNNSs papers, since PMMA can only act as H-bonds acceptors through the ester functional group on the side chain. But our NF-BNNSs-PVA papers belong to multi-H-bonds papers, as PVA can act as both H-bonds acceptors and donors. The mechanical properties of NF-BNNSs-PMMA papers with different PMMA loading are also characterized. As predicted, the mechanical properties of NF-BNNSs-PMMA papers (Figure S8 and Table S1, ESI†) are significantly lower than those of NF-BNNSs-PVA papers with the same NF-BNNSs-polymer mass ratios. For example, at the same polymer loading (6 wt%), the tensile strength, Young's modulus and toughness of NF-BNNSs-PMMA paper are only 12.1±3.8 MPa, 2.6±0.4 GPa, and 0.065±0.04 MJ m^{-3}, respectively. This observation demonstrates that PVA molecules indeed create a network of many H-bonds between stacked NF-BNNSs that can readily enhance the mechanical properties.

Since the mechanical characteristics include mechanical strength, Young's modulus and toughness, the comparison of mechanical characteristics with other analogs is particularly difficult, when one item includes three evaluation indexes. Herein, a radar chart method widely applied to examine one item related with multiple factors,[47, 48] is developed to quantitatively estimate the integrated mechanical performance (IMP) by the volume of triangular pyramid formed as the coordinate data (Figure 4a). The IMPs of NF-BNNSs-PVA paper (6 wt% PVA), its reference (natural nacre), and its analogues (graphene and graphene oxide papers) [9, 11, 34, 35, 37, 49-54] are clearly displayed to compare in Figure 4b. The detailed data of the mechanical characteristics and the calculated volume of triangular pyramid are listed in Table S2. Compared to the high IMP value of natural nacre (11700), the IMP value of our nacre-like paper is only 4659.7. A plausible explanation is that the packing of $CaCO_3$ platelets presents long-range order in natural nacre, but short-range order in our nacre-like paper. On the other hand, our nacre-like paper contains too much soft phase, and the ceramic layer dimension is still somewhat small in comparison to natural nacre. Despite inferior to natural nacre's, the IMP of NF-BNNSs-PVA paper is better than those of its analogues, graphene or graphene oxide papers, indicating a better balance of strength, Young's modulus and toughness for the NF-BNNSs-PVA paper. For graphene or GO papers, the improvement in strength and Young's modulus by covalent or ionic cross-linking usually results in the decreased toughness. For example, the GO paper treated with covalent cross-linking shows a very high strength and Young's modulus (178.9 MPa and 84.8 GPa, respectively), but the toughness is reduced to only 0.02 MJ m^{-3}.[11] On the other hand, selection of polymer and designing the soft interfacial interaction with graphene sheet tends to simultaneously enhance the tensile strength (129.6 MPa) and toughness (3.91 MJ m^{-3}), but the Young's modulus (1.6 GPa) deteriorates.[37]

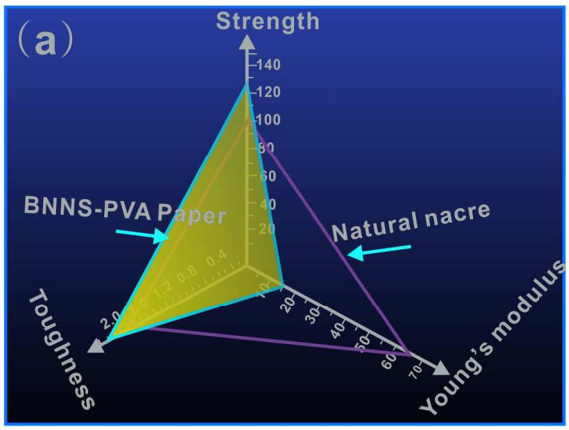

Figure 4. Comparison of mechanical properties of our artificial nacre with natural and the reported graphene and graphene oxide papers. (a) Radar chart presentation of three mechanical parameters for NF-BNNSs-PVA paper and natrual nacre. The volume of triangular pyramid formed by the coordinate data is used to evaluate the integrated mechanical properties. (b) IMP of the NF-BNNSs-PVA paper with the artificial nacre structure, natural nacre, and other GO or GO papers with different cross-linking strategies. Abbreviations: GO paper, graphene oxide paper; GO-PB^-,GO-1-pyrenebutyrate; GO-PVA, GO-poly (vinyl alcohol); PGO-PEI, polydopamine-capped GO-polyetherimide; GO-Borate, GO-$Na_2B_4O_7.10\ H_2O$; RGO-PCDO, RGO-10, 12-pentacosadiyn-1-ol; CRG-GO, chemically reduced graphene-GO; graphene-CF, graphene carbon fiber; Graphene-DOPA, graphene-3,4-dihydroxy-phenylalanine; RGO-PVA;xGTP-Fe, GO-tannic acid -Fe^{3+} ions.

In addition, the continuing miniaturization of electronic devices has aggravated the problems associated with heat dissipation in the electronic industry.[55] Boron nitride-based materials may have the greatest potential applications in electronic industry due to high thermal conductivity of BN.[56] Therefore, the in-plane thermal conductivity of NF-BNNSs-PVA papers was measured using laser flash technique (Figure 5). Measurement details are given in the Electronic Supplementary Information (Figure S9 and Table S3, ESI†). As shown in Figure 5, the thermal conductivity for pure NF-BNNSs-PVA is 4.0 W m^{-1} K^{-1}, and increases as more PVA is added. The thermal conductivity peaks at a PVA loading of 6 wt% (6.9 W m^{-1} K^{-1}) and decrese if more PVA is added, which agrees with the mechanical properties. Phonons defined as quantized lattice vibrations, are considered as the dominant carriers in heat conduction in the composite materials. Phonon scattering, which is mainly due to defects and interface mismatch, plays a key role in the thermal conductivity.[57, 58] As shown in Figure 3b and c, plentiful air gaps among NF-BNNSs are observed in the pure NF-BNNSs paper, which results in increased phonon scattering, and thus showing low thermal conductivity. Adding PVA molecules which interact with NF-BNNSs via H-bonds, would then remove the gaps and bridge the NF-BNNSs, and thus reduces the number of effective phonon scattering centers, leading to the improvement of thermal conductivity. The decrease of thermal conductivity when adding more PVA may be assigned to be the existence of excess PVA without interacting with SC on BNNSs, thereby leading to part isolation of NF-BNNSs.

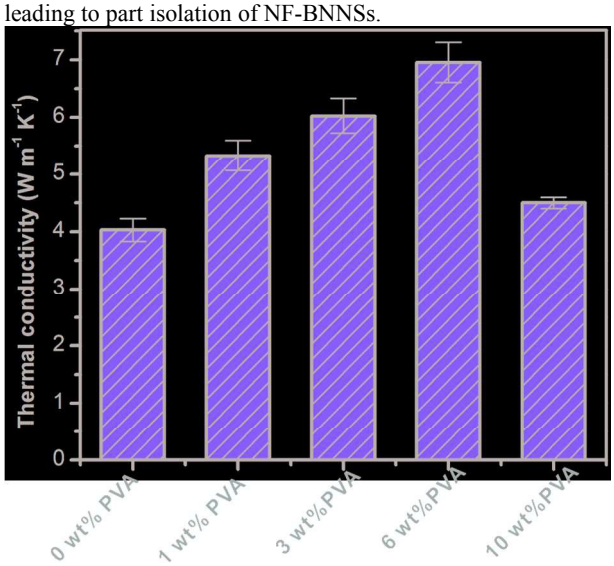

Figure 5. Thermal conductivity of NF-BNNSs-PVA papers with different PVA loadings.

In recent years, flexible electrionics have gained tremendous attention because of the their special features and potential applications in flexible displays, artificial skins, sensors, sustainable energy, etc.[59] To demonstrate the potential application of the materials in flexible electronics, the NF-BNNSs-PVA paper (containing 6 wt % PVA) is utilized as a substrate to fix two light-emitting-diodes (LED) chips by silver paste (Figure 6a). They maintain well working condition under forward (Figure 6b) or reverse (Figure 6c) folding, illustrating excellent flexibility. Polyimides (PIs)[60] and papers[61] have been widely used as substrates for various flexbile electronics, because of their lightweight and high mechanical toughness. However, the thermal conductivity of the common paper (0.03 W m^{-1} K^{-1}) and PIs (0.3 W m^{-1} K^{-1}) is considerably low. In contrast, the NF-BNNSs-PVA paper possesses the unparalleled advantage by the test of thermal imaging camera. After steady-state (10 min) of the same heat flow caused by the equal standard LED chips (Figure 6d), the temperature distribution is uniform for the NF-BNNSs-PVA paper with the satisfactory center spot temperature (34.6 °C, Figure 6e), which will markedly improve the reliability and lifetime of electronics. However, the heat flowed from LED chips are excessive concentrated to generate the hot spots on both common paper (Figure 6f) and PI substrate (Figure 6h), with a

high temperature gradients from the centers to the edges of the samples (Figure 6g and 6i). The highest center spot temperatures for common paper and PI substrates stupendously reach up to 144 °C and 72.3 °C, respectively, obviously tend to reduce the lifetime of the LED chips.

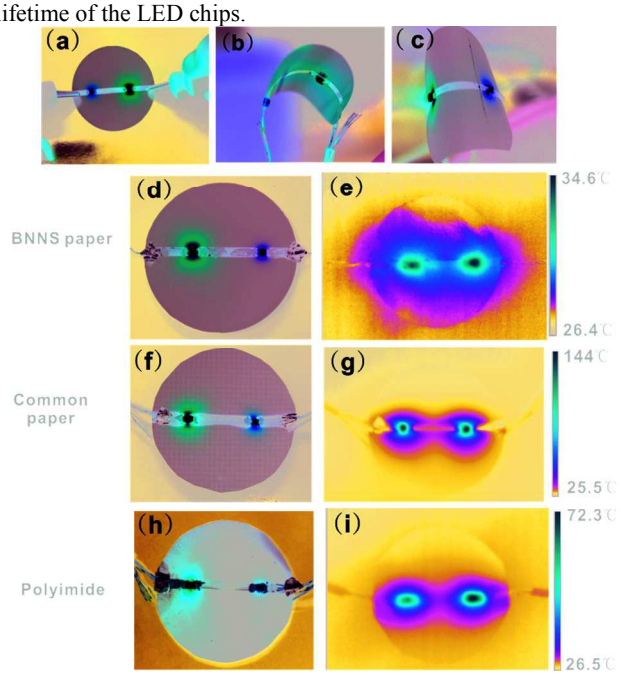

Figure 6. Application of our artificial nacre in flexible substrate. (a-c) Operation of a LED chips on a NF-BNNSs-PVA paper substrate at flat (a), forward (b) and reverse (c) folding. (d, f, and h) Optical images of NF-BNNSs-PVA paper (d), common paper (f), PI (h) substrate. (e, f, and i) The corresponding thermal images of NF-BNNSs-PVA paper (e), common paper (g) and PI (i) recorded by an infrared camera at the same steady-state.

Conclusions

We have demonstrated the fabrication of a new type of artificial nacre-like materials based on NF-BNNSs through vacuum-assisted self-assembly process. The resulting papers have excellent mechanical properties, which is due to the ordered 'brick-and-mortar' arrangement and the unique cross-linking between NF-BNNSs and the PVA via H-bonds. The tensile strength, Young's modulus, and toughness of the NF-BNNSs-PVA paper with 6 wt % PVA are 125.20 MPa, 15.7 GPa, and 2.37 MJ m^{-3}, respectively, which partly surpass natural nacre. The integrated mechanical property of the NF-BNNSs-PVA papers evaluated by radar chart analysis method, is better than that of most of nacre-like papers based on graphene or graphene oxide, demonstrating the excellent balance of tensile strength, Young's modulus, and toughness. The artificial nacre-like papers also exhibit high thermal conductivity (up to 6.9 W m^{-1} K^{-1} for 6 wt % PVA), and reveal the superiority as flexible substrates to support light-emitting-diode (LED) chips. This study opens the door toward biomimetic production of the BNNSs-based composites with excellent mechanical properties and high thermal conductivity, which will have great promising application in flexible devices. Intrinsically insulating NF-BNNSs-PVA papers can also open some applications that are impossible with other electrically conductive papers based on carbon nanotubes and graphene.

Acknowledgements

The authors acknowledge the financial support from Guangdong and Shenzhen Innovative Research Team Program (No. 2011D052 and KYPT20121228160843692), Shenzhen Electronic Packaging Materials Engineering Laboratory (No.2012-372), Research Grants Council of Hong Kong, particularly, via Grant Nos. AoE/P-03/08, N_CUHK405/12, T23-407/13-N, and CUHK Group Research Scheme.

Notes and references

[a]*Shenzhen Institutes of Advanced Technology, Chinese Academy of Sciences. Shenzhen, China. Fax: 86-755-86392299; Tel: 86-755-86392158; Email: rong.sun@siat.ac.cn*

[b] Department of Electronics Engineering, The Chinese University of Hong Kong, Hong Kong, China. Fax: 852-26035558 ; Tel: 852-39438297; Email: *jbxu@ee.cuhk.edu.hk*

‡Xiaoliang Zeng and Lei Ye contributed equally to this work.

† Electronic Supplementary Information (ESI) available: [TEM images of NF-BNNSs, Raman spectra of raw h-BN and BNNSs, TGA curves of raw BN and NF-BNNSs, XRD patterns of NF-BNNSs-PVA paper and pure BNNSs paper, optical images of NF-BNNSs-PVA paper and pure BNNSs paper, TGA curves of NF-BNNSs-PVA papers, stress-strain curves of the NF-BNNSs-PMMA papers as a function of PMMA contents, typical DSC curves of blank, sapphire, and sample to calculate the CP of samples, measurement of in-plane thermal conductivity, summary of the mechanical properties of the papers measured by tensile testing, comparison of mechanical properties of our artificial nacre with the natural nacre and the reported graphene and graphene oxide papers, a summary of the detailed sample information and thermal properties]. See DOI: 10.1039/b000000x/

1. R. S. Singh, R. Y. Tay, W. L. Chow, S. H. Tsang, G. Mallick and E. H. T. Teo, *Appl. Phys. Lett.*, 2014, **104**, 163101.
2. L. H. Li, J. Cervenka, K. Watanabe, T. Taniguchi and Y. Chen, *Acs Nano*, 2014, **8**, 1457-1462.
3. Y. Lin, T. V. Williams, W. Cao, H. E. Elsayed-Ali and J. W. Connell, *J. Phys. Chem. C*, 2010, **114**, 17434-17439.
4. A. Pakdel, C. Zhi, Y. Bando and D. Golberg, *Mater. Today*, 2012, **15**, 256-265.
5. W. Lei, D. Portehault, D. Liu, S. Qin and Y. Chen, *Nat. Commun.*, 2013, **4**.
6. I. Jo, M. T. Pettes, J. Kim, K. Watanabe, T. Taniguchi, Z. Yao and L. Shi, *Nano Lett.*, 2013, **13**, 550-554.
7. D. Golberg, Y. Bando, Y. Huang, T. Terao, M. Mitome, C. Tang and C. Zhi, *Acs Nano*, 2010, **4**, 2979-2993.
8. Y. Lin and J. W. Connell, *Nanoscale*, 2012, **4**, 6908-6939.
9. D. A. Dikin, S. Stankovich, E. J. Zimney, R. D. Piner, G. H. B. Dommett, G. Evmenenko, S. T. Nguyen and R. S. Ruoff, *Nature*, 2007, **448**, 457-460.
10. Y.-L. Zhang, Q.-D. Chen, Z. Jin, E. Kim and H.-B. Sun, *Nanoscale*, 2012, **4**, 4858-4869.
11. Y. Tian, Y. Cao, Y. Wang, W. Yang and J. Feng, *Adv. Mater.*, 2013, **25**, 2980-2983.
12. P. Simek, Z. Sofer, O. Jankovsky, D. Sedmidubsky and M. Pumera, *Adv. Funct. Mater.*, 2014, **24**, 4878-4885.
13. G. Xin, H. Sun, T. Hu, H. R. Fard, X. Sun, N. Koratkar, T. Borca-Tasciuc and J. Lian, *Adv. Mater.*, 2014, **26**, 4521-4526.

14. Q.-Q. Kong, Z. Liu, J.-G. Gao, C.-M. Chen, Q. Zhang, G. Zhou, Z.-C. Tao, X.-H. Zhang, M.-Z. Wang, F. Li and R. Cai, *Adv. Funct. Mater.*, 2014, **24**, 4222-4228.
15. F. Xiao, Y. Li, X. Zan, K. Liao, R. Xu and H. Duan, *Adv. Funct. Mater.*, 2012, **22**, 2487-2494.
16. S.-S. Li, H.-P. Cong, P. Wang and S.-H. Yu, *Nanoscale*, 2014, **6**, 7534-7541.
17. A. B. Dichiara, T. J. Sherwood, J. Benton-Smith, J. C. Wilson, S. J. Weinstein and R. E. Rogers, *Nanoscale*, 2014, **6**, 6322-6327.
18. S.-K. Li, Y.-X. Yan, J.-L. Wang and S.-H. Yu, *Nanoscale*, 2013, **5**, 12616-12623.
19. L. David, R. Bhandavat and G. Singh, *Acs Nano*, 2014, **8**, 1759-1770.
20. C.-B. Ma, X. Qi, B. Chen, S. Bao, Z. Yin, X.-J. Wu, Z. Luo, J. Wei, H.-L. Zhang and H. Zhang, *Nanoscale*, 2014, **6**, 5624-5629.
21. J. N. Coleman, M. Lotya, A. O'Neill, S. D. Bergin, P. J. King, U. Khan, K. Young, A. Gaucher, S. De, R. J. Smith, I. V. Shvets, S. K. Arora, G. Stanton, H.-Y. Kim, K. Lee, G. T. Kim, G. S. Duesberg, T. Hallam, J. J. Boland, J. J. Wang, J. F. Donegan, J. C. Grunlan, G. Moriarty, A. Shmeliov, R. J. Nicholls, J. M. Perkins, E. M. Grieveson, K. Theuwissen, D. W. McComb, P. D. Nellist and V. Nicolosi, *Science*, 2011, **331**, 568-571.
22. Y. Yao, Z. Lin, Z. Li, X. Song, K.-S. Moon and C.-P. Wong, *J. Mater. Chem.*, 2012, **22**, 13494-13499.
23. C. Ortiz and M. C. Boyce, *Science*, 2008, **319**, 1053-1054.
24. U. G. K. Wegst, H. Bai, E. Saiz, A. P. Tomsia and R. O. Ritchie, *Nat Mater*, 2015, **14**, 23-36.
25. F. Bouville, E. Maire, S. Meille, B. Van de Moortele, A. J. Stevenson and S. Deville, *Nat. Mater.*, 2014, **13**, 508-514.
26. E. Munch, M. E. Launey, D. H. Alsem, E. Saiz, A. P. Tomsia and R. O. Ritchie, *Science*, 2008, **322**, 1516-1520.
27. A. P. Jackson, J. F. V. Vincent and R. M. Turner, *P. Roy. Soc. B-Biol. Sci.*, 1988, **234**, 415-440.
28. H.-B. Yao, J. Ge, L.-B. Mao, Y.-X. Yan and S.-H. Yu, *Adv. Mater.*, 2014, **26**, 163-188.
29. Q. Cheng, L. Jiang and Z. Tang, *Acc. Chem. Res.*, 2014, **47**, 1256-1266.
30. J. Wang, Q. Cheng and Z. Tang, *Chem. Soc. Rev.*, 2012, **41**, 1111-1129.
31. D. Zhong, Q. Yang, L. Guo, S. Dou, K. Liu and L. Jiang, *Nanoscale*, 2013, **5**, 5758-5764.
32. L. Huang, C. Li, W. Yuan and G. Shi, *Nanoscale*, 2013, **5**, 3780-3786.
33. S. Park, K.-S. Lee, G. Bozoklu, W. Cai, S. T. Nguyen and R. S. Ruoff, *ACS Nano*, 2008, **2**, 572-578.
34. R.-Y. Liu and A.-W. Xu, *RSC Adv.*, 2014, **4**, 40390-40395.
35. Z. An, O. C. Compton, K. W. Putz, L. C. Brinson and S. T. Nguyen, *Adv. Mater.*, 2011, **23**, 3842-3846.
36. C. Aulin, G. Salazar-Alvarez and T. Lindstrom, *Nanoscale*, 2012, **4**, 6622-6628.
37. Q. Cheng, M. Wu, M. Li, L. Jiang and Z. Tang, *Angew. Chem. Int. Edit.*, 2013, **52**, 3750-3755.
38. J. Wang, Q. Cheng, L. Lin, L. Chen and L. Jiang, *Nanoscale*, 2013, **5**, 6356-6362.
39. D. Lee, S. H. Song, J. Hwang, S. H. Jin, K. H. Park, B. H. Kim, S. H. Hong and S. Jeon, *Small*, 2013, **9**, 2602-2610.
40. R. Jan, P. May, A. P. Bell, A. Habib, U. Khan and J. N. Coleman, *Nanoscale*, 2014, **6**, 4889-4895.
41. F. Liu, X. Mo, H. Gan, T. Guo, X. Wang, B. Chen, J. Chen, S. Deng, N. Xu, T. Sekiguchi, D. Golberg and Y. Bando, *Sci. Rep.*, 2014, **4**.
42. C. Zhi, Y. Bando, C. Tang, H. Kuwahara and D. Golberg, *Adv. Mater.*, 2009, **21**, 2889-2893.
43. R. J. Smith, P. J. King, M. Lotya, C. Wirtz, U. Khan, S. De, A. O'Neill, G. S. Duesberg, J. C. Grunlan, G. Moriarty, J. Chen, J. Z. Wang, A. I. Minett, V. Nicolosi and J. N. Coleman, *Adv. Mater.*, 2011, **23**, 3944-3948.
44. G. Sugihara, D. S. Shigematsu, S. Nagadome, S. Lee, Y. Sasaki and H. Igimi, *Langmuir*, 2000, **16**, 1825-1833.
45. T. Sainsbury, A. Satti, P. May, Z. Wang, I. McGovern, Y. K. Gun'ko and J. Coleman, *J. Am. Chem. Soc.*, 2012, **134**, 18758-18771.
46. Y. Xu, W. Hong, H. Bai, C. Li and G. Shi, *Carbon*, 2009, **47**, 3538-3543.
47. C. Kalonia, O. S. Kumru, J. H. Kim, C. R. Middaugh and D. B. Volkin, *J. Pharm. Sci.*, 2013, **102**, 4256-4267.
48. Y.-C. Chang, C.-J. Chang, K.-T. Chen and C.-L. Lei, *Ieee Network*, 2012, **26**, 25-31.
49. Q.-Q. Kong, Z. Liu, J.-G. Gao, C.-M. Chen, Q. Zhang, G. Zhou, Z.-C. Tao, X.-H. Zhang, M.-Z. Wang, F. Li and R. Cai, *Adv. Funct. Mater.*, 2014, **24**, 4222-4228.
50. K. W. Putz, O. C. Compton, M. J. Palmeri, S. T. Nguyen and L. C. Brinson, *Adv. Funct. Mater.*, 2010, **20**, 3322-3329.
51. K. Shu, C. Wang, M. Wang, C. Zhao and G. G. Wallace, *J. Mater. Chem. A*, 2014, **2**, 1325-1331.
52. Y. Xu, H. Bai, G. Lu, C. Li and G. Shi, *J. Am. Chem. Soc.*, 2008, **130**, 5856-5857.
53. B. Yuan, C. Bao, X. Qian, L. Song, Q. Tai, K. M. Liew and Y. Hu, *Carbon*, 2014, **75**, 178-189.
54. D. Zhong, Q. L. Yang, L. Guo, S. X. Dou, K. S. Liu and L. Jiang, *Nanoscale*, 2013, **5**, 5758-5764.
55. X. Huang, P. Jiang and T. Tanaka, *Ieee Electrical Insulation Magazine*, 2011, **27**, 8-16.
56. X. Huang, S. Wang, M. Zhu, K. Yang, P. Jiang, Y. Bando, D. Golberg and C. Zhi, *Nanotechnology*, 2015, **26**, 015705.
57. A. L. Moore and L. Shi, *Mater. Today*, 2014, **17**, 163-174.
58. X. Huang, T. Iizuka, P. Jiang, Y. Ohki and T. Tanaka, *J. Phys. Chem. C*, 2012, **116**, 13629-13639.
59. Z. Liu, J. Xu, D. Chen and G. Shen, *Chem. Soc. Rev.*, 2015, **44**, 161-192.
60. M.-C. Choi, J. Wakita, C.-S. Ha and S. Ando, *Macromolecules*, 2009, **42**, 5112-5120.
61. W. J. Hyun, O. O. Park and B. D. Chin, *Adv. Mater.*, 2013, **25**, 4729-4734.